Multibeam x-ray optical system for high-speed tomography

Letter

optica

A multi-beam X-ray optical system for high-speed tomography

WOLFGANG VOEGELI,[1,*] KENTARO KAJIWARA,[2] HIROYUKI KUDO,[3] TETSUROH SHIRASAWA,[4] LIANG XIAOYU,[5] AND WATARU YASHIRO[5,*]

[1]Department of Physics, Tokyo Gakugei University, 4-1-1 Nukuikita-machi, Koganei, Tokyo 184-8501, Japan
[2]Japan Synchrotron Radiation Research Institute (JASRI), 1-1-1 Kouto, Sayo, Hyogo 679-5198, Japan
[3]Faculty of Engineering, Information and Systems, University of Tsukuba, 1-1-1 Tennoudai, Tsukuba, Ibaraki 305-8573, Japan
[4]National Metrology Institute of Japan, National Institute of Advanced Industrial Science and Technology, 5-2-2107 1-1-1 Higashi, Tsukuba, Ibaraki 305-8565, Japan
[5]Institute of Multidisciplinary Research for Advanced Materials (IMRAM), Tohoku University, 2-1-1 Katahira, Sendai 980-8577, Japan

*Corresponding authors: wvoegeli@u-gakugei.ac.jp, wataru.yashiro.a2@tohoku.ac.jp

Received XX Month XXXX; revised XX Month, XXXX; accepted XX Month XXXX; posted XX Month XXXX (Doc. ID XXXXX); published XX Month XXXX

X-ray tomography is a powerful method for visualizing the three-dimensional structure of an object with a high spatial resolution. Conventional time-resolved X-ray tomography using synchrotron radiation requires fast rotation of the object, which limits the temporal resolution and hampers its application to, e.g., fluids and in vivo observation of living beings. Here, we present a multi-beam X-ray optical system for high-speed 4D tomography, which can obtain projection images of a sample in a wide angular range simultaneously. It consists of about three dozen single-crystalline blades oriented with different angles to the incident beam, which each Bragg-reflect a part of the incident X-rays in the direction of the sample position. 32 projection images covering an angular range of more than ±70° were obtained without moving the sample or optical system, with an exposure time of 1 ms. The data set was successfully used for reconstructing the three-dimensional structure of two test samples. The optical system provides the basis for realizing millisecond time resolution X-ray tomography of non-repeatable phenomena, and can be expected to be useful for other applications as well, for example for time-resolved element-specific imaging.

http://dx.doi.org/10.1364/optica.99.099999

The interest in dynamical phenomena is increasing in recent years, creating demand in material and life science for visualization of internal structures with high temporal and spatial resolution. X-ray computed tomography (CT) is often the method of choice for analyzing static samples, because it gives three-dimensional information, but it is not easy to obtain data with a time resolution below the sub-seconds range. The reason is that for each time step, a few hundred projection images of the sample at different projection angles are necessary, which are usually obtained either by rotating the sample or by moving the X-ray source and detector around the sample.

This is not a problem for repeatable phenomena, for example sub-millisecond 4D-CT of a blowfly in flight has been reported [1]. Many dynamical phenomena are not repeatable, however, for example the reaction of animals to stimuli, chemical reactions, inelastic mechanical deformations or annealing processes. For these, the temporal resolution is determined by the time needed for acquiring a whole tomographic data set.

Efforts to improve the temporal resolution for phenomena that are difficult to repeat have led to progress recently. The conceptually simplest approach is to increase the speed of the sample rotation and the image acquisition as much as possible. X-ray tomographs with sub-second time-resolution of a polypropylene sphere [2], a living worm [3], lithium-ion batteries [4] and a burning match stick [5] have been obtained, for example. Towards faster time resolutions, X-ray phase tomography with a temporal resolution down to 2 ms has been demonstrated using a white synchrotron radiation source [6, 7, 8]. A similar approach has been used for in-situ tomography of a foaming metal with a temporal resolution of 4.8 ms [9]. The high-speed rotation can pose problems for controlling the environment of the sample and for observing fluids or living animals, however. For example, the radial acceleration due to rotation at 104 Hz has been calculated to be 42 m/s^2 at the edge of a sample with radius 1 mm [9]. The corresponding centrifugal forces will affect the sample in many cases.

A different approach to obtain time-resolved three-dimensional information is to image the sample simultaneously from several directions. Bieberle *et al.* have devised a moving X-ray source by scanning an electron beam and used it to obtain X-ray tomographs with a time resolution of 2 ms, albeit with a spatial resolution of about 1 mm [10]. When a single stationary X-ray source is used, the large deflection angles necessary for this purpose are best achieved using diffraction at single crystals. Hoshino *et al.* have succeeded in stereo and triscopic imaging of a living mouse using a synchrotron radiation beam and one or two Si single crystals [11, 12]. More recently, three projections were

obtained using a single Si crystal, with the potential to obtain 9 projections simultaneously [13]. However, to date the reported setups are limited to a few projections, and are therefore not suitable for tomographic reconstruction.

Here, we present a multi-beam X-ray optical system that creates about 30 X-ray beams from a white synchrotron radiation beam, which can be used to image a sample simultaneously in a wide angular range. The evaluation of the system shows its potential for obtaining data sufficient for tomographic reconstruction with a time resolution of 1 ms. By combination with a system for simultaneous detection of the beams, high-speed 4D tomography without sample rotation could be realized.

The key element of the multi-beam optical system is a thin silicon crystal (multi-blade crystal), whose upper part consists of a number of blades that are connected by a 200 μm-wide bridge to the lower part (Fig. 1 (a)). The lower part of the crystal is bent to the shape of a hyperbola. Each blade takes the orientation of the lower part of the crystal where the bridge is located, but remains flat.

The multi-blade crystal was prepared such that the (110) crystal planes are perpendicular to both the surface and the horizontal plane. When a white X-ray beam is incident onto the crystal, these crystal planes diffract X-rays with energies satisfying the Bragg condition. A hyperbola has the property that radiation emitted from one of its foci, F_1, is reflected towards the second focus F_2 in a Laue geometry. In the present case, a white synchrotron radiation source is located at F_1 and the X-rays reflected at the horizontal center of each blade by the (110) planes pass through F_2. Since each blade is flat, parallel beams are created that can be used for imaging a sample placed at F_2 simultaneously from different directions.

In this setup, the number of beams and their angular spacing is determined by the focal length, the width of the white beam and the width of each crystal blade. To obtain large scattering angles, the focal length must be small. For small scattering angles, that is, near the line connecting its two foci, the curvature radius of the hyperbola becomes small. It is difficult to bent the silicon crystals to the small curvature radii needed to realize a near 180° angular range with the constraints imposed by a typical white synchrotron radiation beam line. In order to achieve both a wide range of scattering angles and a large number of beams, and at the same time avoiding small curvature radii, a total of 4 crystals placed on three crystal benders with different focal distances were used (Fig. 1(b), (c)). Details are given in Supplement 1.

The multi-blade crystals were fabricated from double-side-polished Si(001) wafers (thickness 200 μm). First, grooves 80 μm deep and 200 μm wide, which determine the outlines of the multi-blade crystals, were formed by using a deep reactive ion etching system (MUC-21, Sumitomo Precision Products). Next, the back sides of the wafers were dry-etched uniformly by inductively-coupled plasma to form the multi-blade crystals with a thickness of 80 μm out of the wafers. They were bent by fixing them to aluminum holders machined to the desired hyperbolic shape (Fig, 1 (d)).

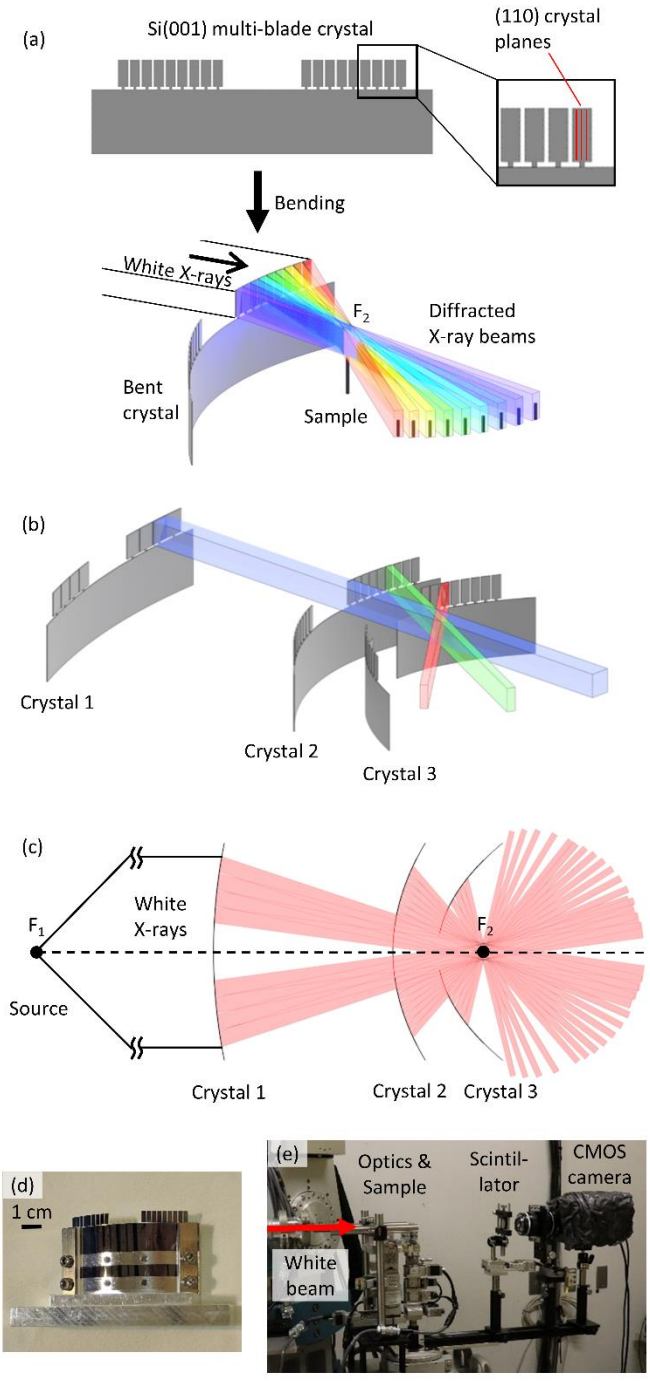

Fig. 1. (a) Principle of the multi-beam optical element. A Si crystal with a number of blades is bent such that the X-ray beams diffracted at each blade converge on the sample position. (b) Schematic illustration of the multi-beam optics consisting of three optical elements with different focal lengths. Only one X-ray beam from each optical element is shown for clarity. (c) Top view of the multi-beam optics showing all measured X-ray beams. (d) Crystal 2 mounted on the crystal bender. (e) Experimental setup.

A proof-of-concept experiment for the multi-beam optical system was performed using bending magnet radiation at beamline 28B2 of SPring-8 (Fig. 1 (e)). This beamline has a photon flux density of about

10^{14} photons/s/mrad^2/0.1%BW in the energy range 10-50 keV [14]. The multi-beam optical system was placed at a distance of 45 m from the source, where the white X-ray beam has a size of 50 mm (H) ×10 mm (V). Two test samples were measured, a tungsten wire (Nilaco, diameter 50 μm) and aluminum tape (Nichiban AL-50, thickness 50 μm) rolled into a cylindrical shape. The diffracted beams from each blade were observed with a detector consisting of a scintillator in combination with an optical lens system and a high-speed CMOS camera (Photron FASTCAM Mini AX100). A 40-μm-thick Gd_2O_2S:Tb scintillator was used for the tungsten wire and a 100-μm-thick Ce:$Gd_3Al_2Ga_3O_{12}$ single crystal [15] for the Al tape sample. The X-ray beams were observed sequentially by positioning the detector appropriately. For the direct beam, a 40 μm-thick Ce:$Gd_3Al_2Ga_3O_{12}$ (Ce:GAGG) scintillator (10 μm thick for the Al tape sample) and a Photron FASTCAM Nova S12 type 1000K CMOS camera was used. The effective pixel sizes of the two cameras were 20 μm×20 μm and 10 μm×10 μm. When using the 40-μm-thick Gd_2O_2S:Tb scintillator, the FWHM of the point spread function of the detector approximated by a Gaussian function was determined to be 65 μm (see Supplement 1).

The samples were placed at the focus position F_2. Images of each X-ray beam were recorded with an exposure time of 1 ms (500 ns for the direct beam). The transmittance T was calculated from the intensities I and I_0 with and without the sample with the readout noise subtracted. 50 images with an exposure time of 1 ms were averaged for I_0.

The tungsten wire is intended as a simple, well-defined sample to spot problems with the tomographic reconstruction that might arise from relative rotations or distortions of the beams. Figure 2 (a) shows a typical transmittance image of the tungsten wire taken with the present setup. The size of this beam is 1.9×3.9 mm^2. In total, 32 transmittance images were observed in the angular range from -73.5° to 77.9°. See Fig. S1 in Supplement 1 for projection images and scattering angles of each beam.

The three-dimensional structure of the sample was reconstructed from the 1 ms-exposure-time transmittance image data by the following procedure. First, the measured transmittance images were converted to the line-integral projection data by a calibration assuming a uniform density and constant diameter for the tungsten wire. Second, a compressed-sensing algorithm using total variation regularization was used for reconstruction from the small number of available projections, *i.e.* 32 projections [16-19]. The successful reconstruction (Fig. 2 (b)) proves that the transmittance images were recorded without distortions and that they could be correctly related to each other. Details of the data analysis, a tomogram and line profiles of the reconstruction are given in Supplement 1.

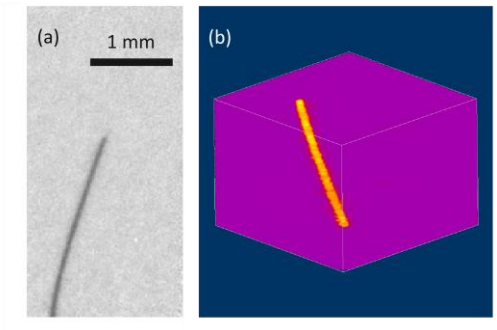

Fig. 2. (a) A typical transmittance image of the tungsten wire sample using the beam with a scattering angle of 32.3°. The exposure time is 1 ms. [gray scale: 0-1.2] (b) Three-dimensional reconstruction of the tungsten wire sample (rendered using Maximum Intensity Projection). The size of the box is 2.56×2.56×1.86 mm^3.

The Al tape sample is a weakly absorbing sample with a more complex shape. An example of a transmittance image is shown in Fig. 3 (a), and a tomogram in Fig. 3 (b). In this case, the transmittance was converted to line-integral projection data using an effective absorption coefficient, which was obtained by measuring the absorption of aluminum films of known thickness. A homogenous composition is assumed for the analysis, but the density or thickness of the sample does not need to be uniform. For the reconstruction, the same compressed-sensing algorithm was used as for the tungsten wire. The topology of the sample, i.e. a hollow cylinder, was correctly reconstructed and a part of the overlapping walls is resolved. The density variation in the walls of the cylinder is likely caused by insufficient signal-noise ratio for the beams with a large scattering angle.

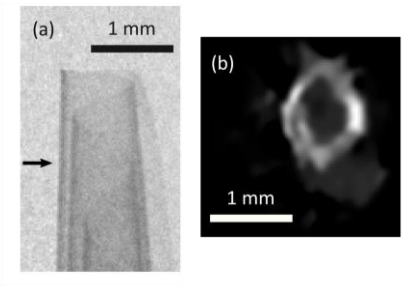

Fig. 3. (a) Transmittance image of the Al tape sample at a scattering angle of 32.3° [gray scale: 0-1.2]. (b) Tomogram of the Al tape sample, at the height indicated by the arrow in (a).

The X-ray energy of each beam is different in the present optical system, since it is determined by the Bragg condition for each crystal blade. The X-ray beams also include higher harmonics in addition to the fundamental Bragg reflection. The absorption depends on the X-ray energy, and the transmittance images must be converted to line-integral projection data on a common scale for absorption tomography. To achieve this, assumptions are necessary, in the case of the Al tape sample that a single effective absorption coefficient can be used and that the composition of the sample is homogeneous.

Grating-based phase-contrast imaging [20-25] would be more suited for quantitative measurements, as the grating interferometer works as an energy band-pass filter, and the energy close to the design energy of the interferometer contributes dominantly. This fact makes the interpretation of a differential-phase image easier: the differential-phase signals in the image are inversely proportional to the energy close to the design energy in a good approximation. In addition, phase-contrast imaging generally has a much higher sensitivity than conventional X-ray absorption-contrast imaging, and enables us to visualize inner structures of materials consisting of light elements. Especially, grating-based imaging can provide three images simultaneously, absorption-contrast, differential-phase, and dark-field images, each of which can be used to obtain quantitative tomograms. Grating-base differential phase imaging has been used in millisecond-order X-ray phase tomography with sample rotation [6], and it should be possible to realize a temporal resolution of a few milliseconds using similar 3-step phase stepping. We have confirmed that the coherence of the diffracted beams is sufficient for phase-contrast imaging using grating-based X-ray interferometry.

The multi-beam X-ray optical system has the potential for 4D tomography with an even higher temporal resolution than 1 ms. For

example, high-flux wigglers have a one order of magnitude higher flux density than a bending magnet of SPring-8. Using sources such as these should make it possible to increase the reflected X-ray intensities and improve the temporal resolution significantly. Introducing strain into the single-crystal blades can also increase the intensities. Thus, our approach should be applicable to observation of non-repeatable phenomena even with temporal resolutions of less than 100 μs.

In order to exploit the potential of the multi-beam optical system, a detection system that is able to observe all projections simultaneously is necessary. We have developed a setup for simultaneous observation of four projections with a single CCD camera [26], so to observe all projections 9 cameras (8 for the diffracted beams and one for the direct beam) are sufficient.

The multi-blade crystals can be expected to have other applications than 4D tomography, as well. For example, they can be used to image a sample at different energies simultaneously, because the X-ray energy of each beam is determined by the Bragg angle that it is diffracted with. This provides a new approach to high-speed element-specific X-ray imaging or chemical imaging.

In conclusion, a multi-beam X-ray optical system was developed that can be used to obtain projection images in a wide angular range simultaneously. Using a white synchrotron radiation source from a bending magnet at SPring-8, exposure times of 1 ms were sufficient to image two test sample, a tungsten wire and a hollow aluminum cylinder. This optical system could be used to realize high-speed X-ray tomography by combination with a detection system that can observe all beams simultaneously. Such a system would be able to provide the three-dimensional sample structure with millisecond temporal resolution, without the need to move any part of the experimental setup during the measurement.

Funding. Japan Science and Technology Agency (JST) CREST (JPMJCR1765)**.**

Acknowledgment. The authors thank Prof. Etsuo Arakawa for help with the experiments and fruitful discussions, and Prof. Toshio Takahashi for helpful suggestions. Experiments were conducted at beamline 28B2 of SPring-8. The multi-blade crystals were fabricated at Micro System Integration Center (μSIC) and Technical Support Center, Tohoku University. The holders for the multi-blade crystals were fabricated in the machine shop of IMRAM, Tohoku University. A part of this work was conducted at the National Institute of Advanced Industrial Science and Technology (AIST), supported by "Nanotechnology Platform Program" of the Ministry of Education, Culture, Sports, Science and Technology (MEXT), Japan, Grant Number JPMXP09F19AT0107.

Disclosures. The authors declare no conflicts of interest

See Supplement 1 for supporting content.

REFERENCES

1. S.M. Walker, D.A. Schwyn, R. Mokso, M. Wicklein, T. Müller, M. Doube, M. Stampanoni, H. G. Krapp, G. K. Taylor, PLOS Biology **12,** e1001823 (2014).
2. A. Momose, W. Yashiro, H. Maikusa, and Y. Takeda, Opt. Express **17**, 12540 (2009).
3. A. Momose, W. Yashiro, S. Harasse, and H. Kuwabara, Opt. Express **19,** 8423 (2011).
4. D. P. Finegan, M. Scheel, J. B. Robinson, B. Tjaden, I. Hunt, T. J. Mason, J. Millichamp, M. Di Michiel, G. J. Offer, G. Hinds, D. J.L. Brett and P. R. Shearing, Nat. Commun. **6**, 6924 (2015).
5. A. Ruhlandt, M. Töpperwien, M. Krenkel, R. Mokso and T. Salditt, Scientific Reports, **7**, 6487 (2017).
6. W. Yashiro, C. Kamezawa, D. Noda, and K. Kajiwara, Appl. Phys. Express **11**, 122501 (2018).
7. W. Yashiro, R. Ueda, K. Kajiwara, and D. Noda, Jpn. J. Appl. Phys. **56**, 112503 (2017).
8. W. Yashiro, D. Noda, and K. Kajiwara, Appl. Phys. Express **10**, 052501 (2017).
9. F. García-Moreno, P.H. Kamm, T.R. Neu, F. Bülk, R. Mokso, C. M. Schlepütz, M. Stampanoni, and J. Banhart, Nat Commun **10**, 3762 (2019).
10. M. Bieberle, F. Barthel, H.-J. Menz, H.-G. Mayer, and U. Hampel, Appl. Phys. Lett. **98**, 034101 (2011).
11. M. Hoshino, K. Uesugi, J. Pearson, T. Sonobe, M. Shirai and N. Yagi, J. Synchrotron Rad. **18**, 569 (2011).
12. M. Hoshino, T. Sera, K. Uesugi and N. Yagi, Journal of Instrumentation **8**, C05002 (2013).
13. P. Villanueva-Perez, B. Pedrini, R. Mokso, P. Vagovic, V. A. Guzenko, S. J. Leake, P. R. Willmott, P. Oberta, C. David, H. N. Chapman, and M. Stampanoni, Optica **5**, 1521 (2018).
14. SPring-8, "Bending Magnet", http://www.spring8.or.jp/en/about_us/whats_sp8/facilities/bl/sources/bending_magnet/
15. K. Kamada, T. Endo, K. Tsutumi, T. Yanagida, Y. Fujimoto, A. Fukabori, A. Yoshikawa, J. Pejchal, M. Nikl, Crystal Growth & Design **11**, 4484 (2011).
16. E. Y. Sidky and X. Pan, Phys. Med. Biol. **53**, 4777 (2008).
17. M. Defrise, C. Vanhove, and X. Liu, Inverse Probl. **27**, 065002 (2011).
18. H. Kudo, F. Yamazaki, T. Nemoto, and K. Takaki, Proc. SPIE **9967**, 996711 (2016).
19. T. Wang, H. Kudo, F. Yamazaki, and H. Liu, Phys. Med. Biol. **64**, 145006 (2019).
20. C. David, B. Nohammer, and H. H. Solak, Appl. Phys. Lett. **81**, 3287 (2002).
21. A. Momose, S. Kawamoto, I. Koyama, Y. Hamaishi, K. Takai, and Y. Suzuki, Jpn. J. Appl. Phys. **42**, L866 (2003).
22. T. Weitkamp, A. Diaz, C. David, F. Pfeiffer, M. Stampanoni, P. Cloetens, and E. Ziegler, Opt. Express **13**, 6296 (2005).
23. F. Pfeiffer, T. Weitkamp, O. Bunk, and C. David, Nat. Phys. **2**, 258-261 (2006).
24. F. Pfeiffer, T. Weitkamp, O. Bunk, and C. David, Nat. Mater. **7**, 134 (2008).
25. W. Yashiro, Y. Terui, K. Kawabata, and A. Momose, Opt. Express **18**, 16890 (2010).
26. W. Yashiro, T. Shirasawa, C. Kamezawa, W. Voegeli, E. Arakawa, and K. Kajiwara, Jpn. J. Appl. Phys. **59**, 038003 (2020).

FULL REFERENCES

1. S.M. Walker, D.A. Schwyn, R. Mokso, M. Wicklein, T. Müller, M. Doube, M. Stampanoni, H. G. Krapp, G. K. Taylor, In Vivo Time-Resolved Microtomography Reveals the Mechanics of the Blowfly Flight Motor, PLOS Biology **12,** e1001823 (2014).
2. A. Momose, W. Yashiro, H. Maikusa, and Y. Takeda, "High-speed X-ray phase imaging and X-ray phase tomography with Talbot interferometer and white synchrotron radiation", Opt. Express **17**, 12540-12545 (2009).
3. A. Momose, W. Yashiro, S. Harasse, and H. Kuwabara, "Four-dimensional X-ray phase tomography with Talbot interferometry and white synchrotron radiation: dynamic observation of a living worm", Opt. Express **19,** 8423-8432 (2011).
4. D. P. Finegan, M. Scheel, J. B. Robinson, B. Tjaden, I. Hunt, T. J. Mason, J. Millichamp, M. Di Michiel, G. J. Offer, G. Hinds, D. J.L. Brett and P. R. Shearing, In-operando high-speed tomography of lithium-ion batteries during thermal runaway, Nat. Commun. **6**, 6924 (2015).
5. A. Ruhlandt, M. Töpperwien, M. Krenkel, R. Mokso and T. Salditt, Four dimensional material movies: High speed phase-contrast tomography by

backprojection along dynamically curved paths, Scientific Reports, **7**, 6487 (2017).
6. W. Yashiro, C. Kamezawa, D. Noda, and K. Kajiwara, Millisecond-order X-ray phase tomography with a fringe-scanning method, Appl. Phys. Express **11**, 122501 (2018).
7. W. Yashiro, R. Ueda, K. Kajiwara, and D. Noda, Millisecond-order X-ray phase tomography with compressed sensing, Jpn. J. Appl. Phys. **56**, 112503 (2017).
8. W. Yashiro, D. Noda, and K. Kajiwara, Sub-10-ms X-ray tomography using a grating interferometer, Appl. Phys. Express **10**, 052501 (2017).
9. F. García-Moreno, P.H. Kamm, T.R. Neu, F. Bülk, R. Mokso, C. M. Schlepütz, M. Stampanoni, and J. Banhart, Using X-ray tomoscopy to explore the dynamics of foaming metal, Nat Commun **10**, 3762 (2019) doi:10.1038/s41467-019-11521-1
10. M. Bieberle, F. Barthel, H.-J. Menz, H.-G. Mayer, and U. Hampel, Ultrafast three-dimensional x-ray computed tomography, Appl. Phys. Lett. **98**, 034101 (2011).
11. M. Hoshino, K. Uesugi, J. Pearson, T. Sonobe, M. Shirai and N. Yagi, Development of an X-ray real-time stereo imaging technique using synchrotron radiation, J. Synchrotron Rad. **18**, 569-574 (2011).
12. M. Hoshino, T. Sera, K. Uesugi and N. Yagi, Development of X-ray triscopic imaging system towards three-dimensional measurements of dynamical samples, Journal of Instrumentation **8**, C05002--C05002 (2013). Doi:10.1088/1748-0221/8/05/c05002
13. P. Villanueva-Perez, B. Pedrini, R. Mokso, P. Vagovic, V. A. Guzenko, S. J. Leake, P. R. Willmott, P. Oberta, C. David, H. N. Chapman, and M. Stampanoni, "Hard x-ray multi-projection imaging for single-shot approaches," Optica **5**, 1521-1524 (2018).
14. SPring-8, "Bending Magnet", http://www.spring8.or.jp/en/about_us/whats_sp8/facilities/bl/sources/bending_magnet/
15. K. Kamada, T. Endo, K. Tsutumi, T. Yanagida, Y. Fujimoto, A. Fukabori, A. Yoshikawa, J. Pejchal, M. Nikl, Composition Engineering in Cerium-Doped $(Lu,Gd)_3(Ga,Al)_5O_{12}$ Single-Crystal Scintillators, Crystal Growth & Design **11**, 4484-4490 (2011).
16. E. Y. Sidky and X. Pan, Image reconstruction in circular cone-beam computed tomography by constrained, total-variation minimization, Phys. Med. Biol. **53**, 4777- 4807 (2008).
17. M. Defrise, C. Vanhove, and X. Liu, An algorithm for total variation regularization in high-dimensional linear problems, Inverse Probl. **27**, 065002 (2011).
18. H. Kudo, F. Yamazaki, T. Nemoto, and K. Takaki, A very fast iterative algorithm for TV-regularized image reconstruction with applications to low-dose and few-view CT, Proc. SPIE **9967**, 996711 (2016).
19. T. Wang, H. Kudo, F. Yamazaki, H. Liu, A fast regularized iterative algorithm for fan-beam CT reconstruction, Phys. Med. Biol. **64**, 145006 (2019).
20. C. David, B. Nohammer, and H. H. Solak, Differential x-ray phase contrast imaging using a shearing interferometer, Appl. Phys. Lett. **81**, 3287 (2002).
21. A. Momose, S. Kawamoto, I. Koyama, Y. Hamaishi, K. Takai, and Y. Suzuki, Demonstration of X-Ray Talbot Interferometry, Jpn. J. Appl. Phys. **42**, L866 (2003).
22. T. Weitkamp, A. Diaz, C. David, F. Pfeiffer, M. Stampanoni, P. Cloetens, and E. Ziegler, Differential x-ray phase contrast imaging using a shearing interferometer, Opt. Express **13**, 6296 (2005).
23. F. Pfeiffer, T. Weitkamp, O. Bunk, and C. David, Phase retrieval and differential phase-contrast imaging with low-brilliance X-ray sources, Nat. Phys. **2**, 258-261 (2006).
24. F. Pfeiffer, T. Weitkamp, O. Bunk, and C. David, Hard-X-ray dark-field imaging using a grating interferometer, Nat. Mater. **7**, 134-137 (2008).
25. W. Yashiro, Y. Terui, K. Kawabata, and A. Momose, On the origin of visibility contrast in x-ray Talbot interferometry, Opt. Express **18**, 16890-16901 (2010).
26. W. Yashiro, T. Shirasawa, C. Kamezawa, W. Voegeli, E. Arakawa, and K. Kajiwara, A multi-beam X-ray imaging detector consisting of branched optical fiber bundle, Jpn. J. Appl. Phys. **59**, 038003 (2020).